Available online at www.sciencedirect.com
SCIENCE DIRECT
Journal of Sound and Vibration 293 (2006) 547–556
JOURNAL OF SOUND AND VIBRATION
www.elsevier.com/locate/jsvi

Localization of aerodynamic noise sources of Shinkansen trains

K. Nagakura*

Railway Technical Research Institute, 2-8-38, Hikari-cho, Kokubunji, Tokyo, Japan

Accepted 26 August 2005
Available online 7 February 2006

Abstract

Shinkansen noise consists of various noise sources, such as the rolling noise, concrete bridge structure noise, aerodynamic noise and so on. Among these, the aerodynamic noise is the most important at speeds over 270 km/h in some cases because of its strong dependence on train speed. Thus it is necessary to clarify the characteristics of the aerodynamic noise generated by high speed trains for noise reduction. In this paper, wind tunnel tests using a 1/5 scale Shinkansen train model were performed. An acoustic mirror, which consists of an omni-directional microphone and a reflector, was chosen as a measuring device. First, the principle and characteristics of the acoustic mirror are discussed and a method of estimating quantitatively the aerodynamic noise generated by each part of the model is proposed on the basis of wind tunnel test data. Next, the distribution of aerodynamic noise sources generated by the 1/5 scale Shinkansen train model is shown, based on which the contribution of individual noise sources of Shinkansen trains to the wayside noise level is estimated. Finally, the noise source distribution of real Shinkansen trains was measured with the acoustic mirror in a field test. The results of the field test show a good agreement with those of the wind tunnel tests.

1. Introduction

Shinkansen noise consists of various noise sources, such as the rolling noise, concrete bridge structure noise, aerodynamic noise and so on. Among these, the aerodynamic noise is the most important at speeds over 270 km/h in some cases because of its strong dependence on train speed [1,2]. Thus it is necessary to clarify the characteristics of the aerodynamic noise generated by high speed trains for noise reduction. The wind tunnel test is one of the most useful measures for the purpose. The Railway Technical Research Institute (RTRI) constructed a small-scale wind tunnel at Kokubunji, Tokyo, in 1993, and a large-scale low-noise wind tunnel at Maibara (Maibara Wind Tunnel, MWT) in 1996 [3]. By using these facilities, experiments concerned with the noise generated by high speed trains were carried out, the results of which were utilized for the localization of the noise sources and the reduction of aerodynamic noise [2,3].

In this paper, wind tunnel tests using a 1/5 scale Shinkansen train model performed at MWT are described. An acoustic mirror, which consists of an omni-directive microphone and a reflector, was chosen as a measuring device. First, the principle and characteristics of the acoustic mirror are discussed and a method of estimating quantitatively the aerodynamic noise generated by each part of the model is proposed on the basis

*Tel./fax: +81 42 573 7353.
E-mail address: naga@rtri.or.jp.

0022-460X/$ - see front matter © 2006 Elsevier Ltd. All rights reserved.
doi:10.1016/j.jsv.2005.08.043

of wind tunnel test data. Next the distribution of aerodynamic noise sources generated by the 1/5 scale Shinkansen train model is shown based on which the contribution of individual noise sources of Shinkansen train to the wayside noise level is estimated. Finally, the noise source distribution of Shinkansen trains was measured with the acoustic mirror in a field test in order to validate the results of the wind tunnel test.

2. Wind tunnel tests

2.1. Test set-up

Wind tunnel tests using a 1/5 scale Shinkansen train model were performed in the $2.5 \times 3.0\,\mathrm{m}^2$ open cross section of MWT. The model was set on a supporting floor (see Fig. 1). In order to simulate the flow profile under the car body, the distance between the scaled model and the floor was set to be 160 mm, which corresponds to twice the distance between real Shinkansen trains and the ground [2]. In the experiment, the pantograph noise was omitted from our target, which is one of the strongest sources of aerodynamic noise of Shinkansen trains, because it can be estimated more precisely by tests using a real pantograph. The surface of the Shinkansen train model was divided into several noise source areas. The noise source distribution within each area was measured by traversing an acoustic mirror with an elliptic shape across it. Details of the measuring device will be explained in the next section.

2.2. Measurement techniques

2.2.1. Principle of acoustic mirror [4]

Fig. 2 shows the layout and the coordinate system of a noise source, omni-directional microphone and mirror. Here S and S' denote the front and back surfaces of the mirror; $P(\mathbf{r})$ denotes the pressure field on this configuration; $P_i(\mathbf{r})$ denotes the pressure field of free space; $\mathbf{r}_m$ is the position of the microphone; and $\mathbf{r}$ is a point on the mirror surface. The normal $\mathbf{n}_0$ directs to the medium. When the Green's theorem is applied, the pressure at the microphone position $P(\mathbf{r}_m)$ is obtained by

$$P(\mathbf{r}_m) = P_i(\mathbf{r}_m) + \iint_{(s+s')} P(\mathbf{r}) \frac{\partial}{\partial \mathbf{n}_0} G(\mathbf{r}_m, \mathbf{r})\, \mathrm{d}^2\mathbf{r}. \tag{1}$$

Here G is the free space Green's function given by $G(\mathbf{r}_m, \mathbf{r}) = \exp(\mathrm{i}kR_m)/4\pi R_m$, where k is the wavenumber and R_m is the distance between the microphone and the mirror surface. The unknown pressure field $P(\mathbf{r})$ is approximated by $2P_i(\mathbf{r})$ on the front surface S and by 0 on the back surface S', if the wavelength is sufficiently smaller than the diameter of the mirror. In this frequency range, the incident field term $P_i(\mathbf{r}_m)$ can also be ignored. With these approximations, Eq. (1) is replaced by

$$P(\mathbf{r}_m) = -\frac{1}{2\pi} \iint_{s} P_i(\mathbf{r}) \frac{\mathrm{e}^{\mathrm{i}kR_m}}{R_m} \left(\mathrm{i}k - \frac{1}{R_m}\right) \cos\theta(\mathbf{r})\, \mathrm{d}^2\mathbf{r}. \tag{2}$$

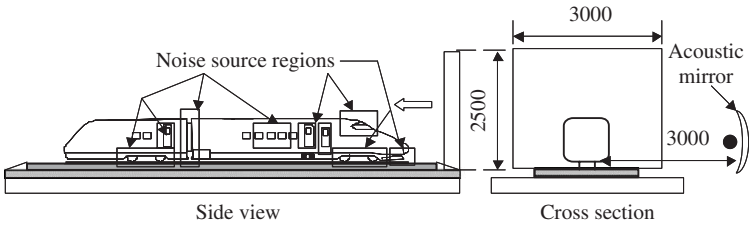

Fig. 1. Test set-up of wind tunnel test using 1/5 scale model of Shinkansen train.

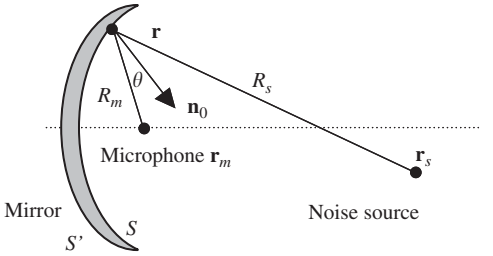

Fig. 2. Layout of mirror, noise source and microphone.

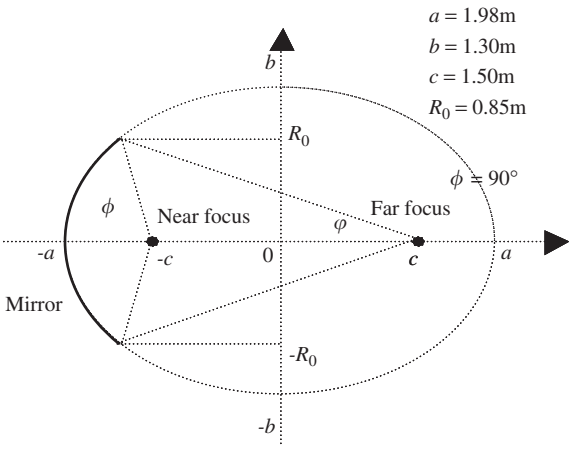

Fig. 3. Mirror geometry.

If the noise source is a monopole type point source whose amplitude of the mass-flux rate is m, Eq. (2) is reduced to

$$P(\mathbf{r}_m) = -\frac{m}{8\pi^2}\iint_S \frac{e^{ik(R_m+R_s)}}{R_m R_s}\left(ik - \frac{1}{R_m}\right)\cos\theta(\mathbf{r})\,d^2\mathbf{r}. \tag{3}$$

Here $\mathbf{r}_s$ is the position of the sound source and R_s is the distance between the sound source and the mirror surface. All calculations shown in this paper are based on Eq. (3).

An acoustic mirror with an elliptic shape is used at MWT. The diameter and focal distance of the mirror is 1.7 and 3 m, respectively (see Fig. 3). A 1/4″ condenser microphone is installed at the near focus with its membrane facing the mirror surface. If a noise source is set at the far focus, the sound path length $R_m + R_s$ is constant for all points on the surface S and a high gain is obtained as a result. As the noise source moves away from the focus in the direction perpendicular to the mirror axis, the variance of the sound path length $R_m + R_s$ due to the position $\mathbf{r}$ increases, and thus the microphone signal drops off due to interference (see Fig. 4, which is referred to the "directivity pattern"). The spatial resolution of the mirror is characterized by the displacement of the source position at which the microphone signal drops off by a given relative amount, such as 10 dB, which is referred to as the "resolution width". A narrower resolution width and higher gain factor are desirable in order to obtain a detailed sound source map.

2.2.2. Characteristics of acoustic mirror in experiments

The characteristics of the acoustic mirror were verified experimentally. A point source was installed in a flow as a calibration noise source [5]. The directivity patterns of the acoustic mirror were obtained by measuring the noise from the point source with the mirror moving parallel to the flow. A typical set of experimental data is shown in Fig. 5, which shows the directivity patterns at different wind velocities for the 1/3-octave band with

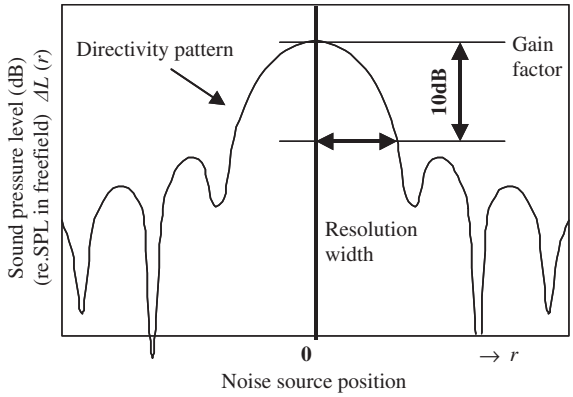

Fig. 4. Definition of directivity pattern.

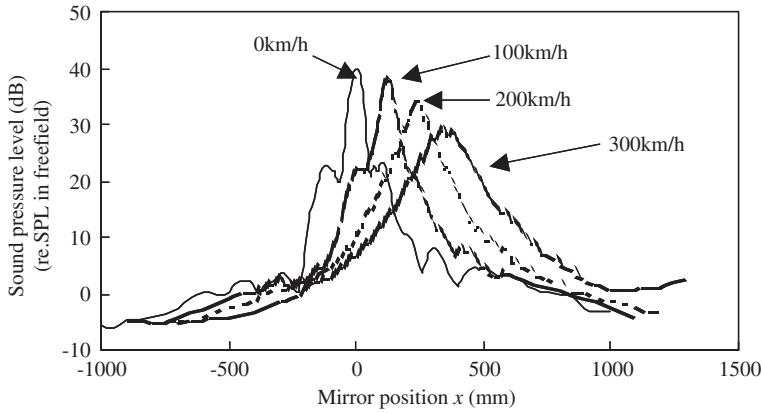

Fig. 5. Directivity patterns of the acoustic mirror obtained experimentally (1/3-octave band with centre frequency $f = 20\,\text{kHz}$).

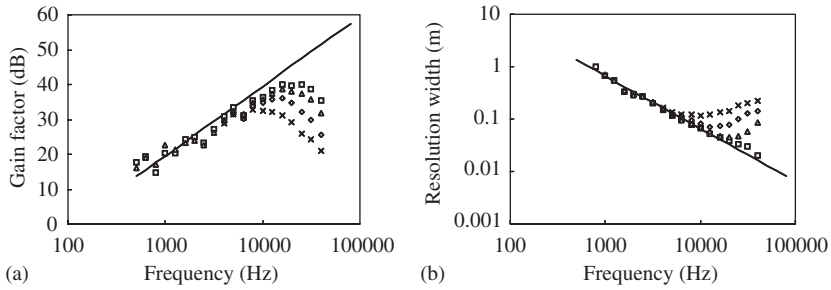

Fig. 6. Characteristics of the acoustic mirror at different wind velocities. □, $U = 0\,\text{km/h}$; △, $U = 100\,\text{km/h}$; ◇, $U = 200\,\text{km/h}$; ×, $U = 300\,\text{km/h}$; —, calculation. (a) Gain factor, (b) resolution width.

the centre frequency 20 kHz. It is found that the maxima of the directivity patterns move in the downstream direction with increasing wind velocity. This is due to the convection of the sound waves. The displacement Δx of the maximum of the directivity pattern is approximated by $\Delta x = Mh$, where M denotes the mach number of the main flow velocity U and h denotes the distance between the point source and the shear layer.

The gain factor and resolution width of the acoustic mirror plotted over the 1/3-octave band frequencies for different wind velocities are shown in Fig. 6. For the wind velocity $v = 0$, the experimental gain factor and resolution width almost agree with the calculated values. However, both the gain factor and resolution width separate from the calculated values when the wind velocity increases, at higher frequencies in particular. This

is mainly due to the scattering of sound waves at the shear layer, which is considerable if the wavelength of the sound wave is smaller than the thickness of shear layer. The resolution width is narrower than 0.5 m above 1 kHz for any wind velocity conditions, which means that the acoustic mirror gives reliable sound source distributions at those frequencies.

2.3. Method of estimation of sound pressure level of real trains

When the sound pressure level of the aerodynamic noise generated by a scaled model is measured with an omni-directional microphone, the sound pressure level in the corresponding field test can be estimated by using the aeroacoustical similarity law, which is summarized by the following equations [2]:

$$f = (l'U/lU')f, \tag{4}$$

$$L(f) = L'(f') + 20\log(r'l/rl') + 10n\log(U/U'). \tag{5}$$

Here f, $L(f)$, l, r, and U are the values in field tests which denote the frequency, frequency spectral density level of the sound intensity, scale of the model, distance between the source and measuring point, and flow velocity, respectively. The primed values are those in the wind tunnel tests. The parameter n denotes the dependence of the sound power on the flow velocity, which is known to be 6 in most cases of the aeroacoustic phenomena on railway trains. Now we have to notice that Eqs. (4) and (5) do not hold in terms of U in some cases, where the acoustical resonance phenomena occur, for example.

When the aerodynamic noise level is estimated quantitatively on the basis of the data measured with the acoustic mirror, its characteristics have to be taken into consideration in addition to applying the similarity law [5]. The characteristics of the acoustic mirror for a point source were examined in Section 2.2.2. However, the acoustic mirror is usually used to determine noise radiation from source distributions in a region under consideration, rather than that from a single point source. This is because the correlation length of the flow-induced sound sources is the scale of the hydrodynamic wavelength, which is smaller than both of the size of the source region and the resolution width of the acoustic mirror. In order to account for the directivity pattern $\Delta L(r)$ in estimating the radiation from the source region, a noise source model of uncorrelated monopole type point sources is introduced. Let a total number of N point sources be distributed homogeneously in a predefined noise source region (S_{source}, the area of which is referred to as S_{area}), which is isolated from other noise source regions, and let the sound power level of each point source be PWL (see Fig. 7). When the sound radiated from the region is measured with the acoustic mirror at its centre, the measured value L_{meas} is denoted by the summation of the contributions of the point sources. Then the sound

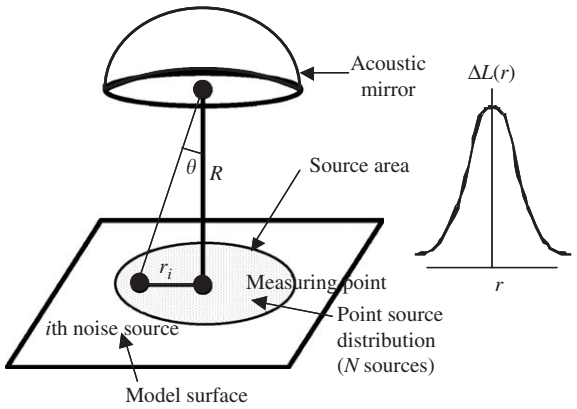

Fig. 7. Noise source model for estimating sound pressure level at far field.

power level PWL is calculated inversely by the following equation:

$$PWL = L_{\text{meas}} - 10\log\left[\frac{1}{2\pi R^2}\sum_{i}^{N} 10^{\Delta L(r_i)/10}\right], \tag{6}$$

where R is the distance between the microphone and source surface and r_i is the distance between the measuring point and the ith source. Eq. (6) can be rewritten as a surface integral on S_{source}:

$$PWL = L_{\text{meas}} - 10\log\left[\frac{1}{2\pi R^2}\frac{N}{S_{\text{area}}}\iint_{S_{\text{source}}} 10^{\Delta L(r)/10}\,\mathrm{d}S\right], \tag{7}$$

where r is the distance between the measuring point and a point on S_{source}. In Eq. (7), the total sound power level of the region, which can be calculated as $PWL + 10\log(N)$, no longer depends on N. Instead, the remaining problem is to specify the relevant source region S_{source}, which can be approximately estimated by the geometric dimensions of the component under consideration.

Once the sound power level is obtained, the sound pressure level at the far field measured with an omni-directional microphone L_{far} is readily estimated by

$$L_{\text{far}} = 10\log\left[\sum_{i}^{N}\left(\frac{10^{\text{PWL}/10}}{2\pi R^2}\right)\right]. \tag{8}$$

If the noise source has the directivity of a dipole whose axis is perpendicular to the source surface, which is often the case in aeroacoustics, the estimated sound power level is not correct because the directivity pattern used in Eqs. (6) and (7) is that for a non-directive point source. However, if the size of the source region is sufficiently smaller than R, the directivity factor $\cos^2\theta$, where θ denotes the incident angle of sound shown in Fig. 7, nearly equals 1, and thus the error in Eqs. (6) and (7) is so small that the directivity shall be considered only in Eq. (8).

2.4. Results of wind tunnel test using 1/5 scale model of Shinkansen trains

Fig. 8 shows typical results of noise source distributions obtained by the experiment. The value at each point on the maps corresponds to the measured one at a particular focus point. Detailed maps of noise source

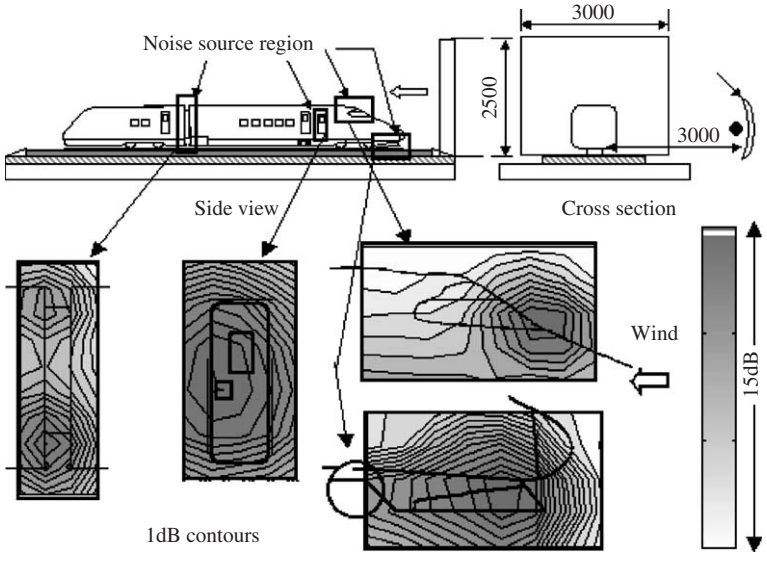

Fig. 8. Noise source distribution of 1/5 scale Shinkansen train model measured with acoustic mirror (1 kHz band (full scale equivalent)).

strength were obtained, the spatial accuracy of which is of the order of 10 cm in model scale. Here it should be noted that the flow around the car body in the wind tunnel test is not exactly the same as that in the case of real train running because of the difference in the Reynolds number, thickness of boundary layer, ground effects and other factors. These figures provide us with the following information in terms of noise sources of Shinkansen trains:

(a) The lower part of the leading car is a strong noise source, which is due to a shear flow at the snowplough.
(b) The noise source of the upper part of leading car concentrates at the position of the wiper, at high frequencies in particular.
(c) The door of the driving cab is a considerably strong noise source at frequencies 500–1000 Hz, which is mainly generated by the handle of the door.
(d) Gaps between adjacent cars generate aerodynamic noise, which is mitigated by the external diaphragm.

Next the noise generated by each area was estimated quantitatively in accordance with the method proposed in Section 2.3. In order to investigate the validity of the method, the frequency spectrum of the noise generated by the lower part of the leading car were calculated by applying Eqs. (6) and (7) to the values measured with the acoustic mirror and compared with that measured with an omni-directive microphone. Both noise levels obtained through the wind tunnel test were converted into the values of the real scale at a point 25 m away from the track by Eqs. (4) and (5). The result is shown in Fig. 9, which suggests the validity of the method. Fig. 10 shows the estimated values of the contribution of individual noise sources to the noise level at a point 25 m away from the track (train velocity 300 km/h). It is found that the lower part of the leading car is the strongest noise source, which is followed by the door for the driving cab, bogies and gaps between cars. However, when a train set, which consists of multiple cars runs on a track with sound barriers, all noise sources in the train set shall be taken into consideration along with the attenuation by sound barriers, and thus the gaps between upper parts of cars become the most prominent noise sources.

3. Field tests

3.1. Measurement techniques

A measurement of the noise source distribution of real trains was conducted with the acoustic mirror on a Shinkansen line. The test set-up is shown in Fig. 11. In the measurement, another acoustic mirror, whose diameter and focal distance are 1.8 m and 5 m, respectively, was used because it was not possible to set a mirror too close to high-speed trains. Above 500 Hz, the resolution width of the mirror is narrower than 1 m,

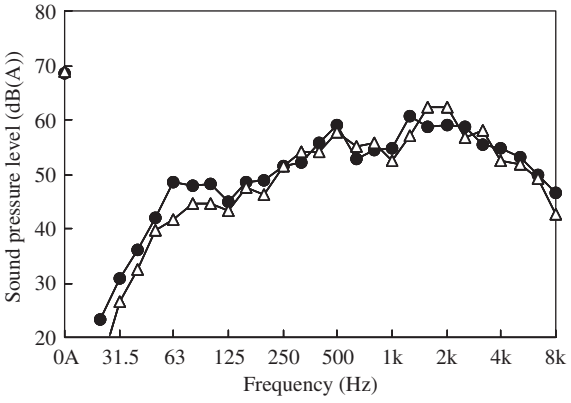

Fig. 9. Frequency spectra of A-weighted sound pressure generated by lower parts of leading car estimated on the basis of results of 1/5 scale model wind tunnel test (full scale equivalent frequency, $U = 200$ km/h, predicted at a point 25 m away from the track), ●, estimated value based on data measured with ellipsoidal apparatus; △, estimated value based on data measured with omni-directional microphone.

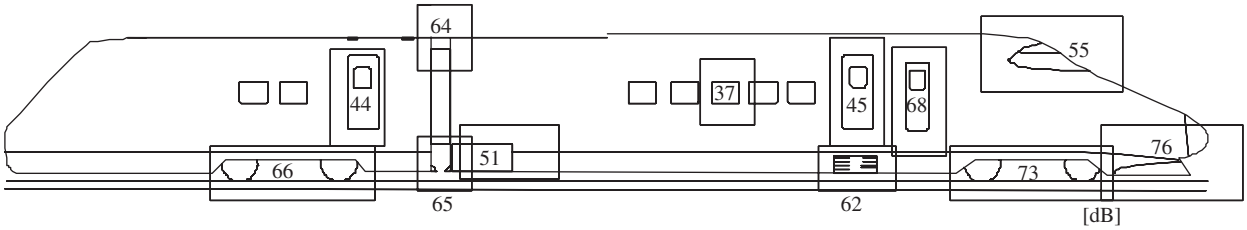

Fig. 10. Estimated sound pressure level of noise generated by individual parts of Shinkansen train ($U = 300\,\mathrm{km/h}$, measured at a point 25 m away from the track without sound barriers).

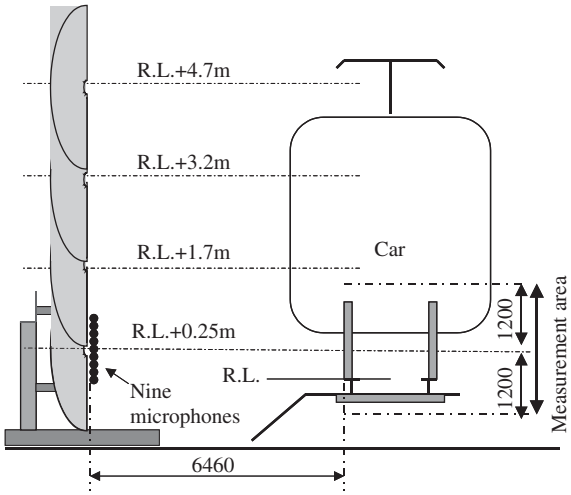

Fig. 11. Test set-up of field test.

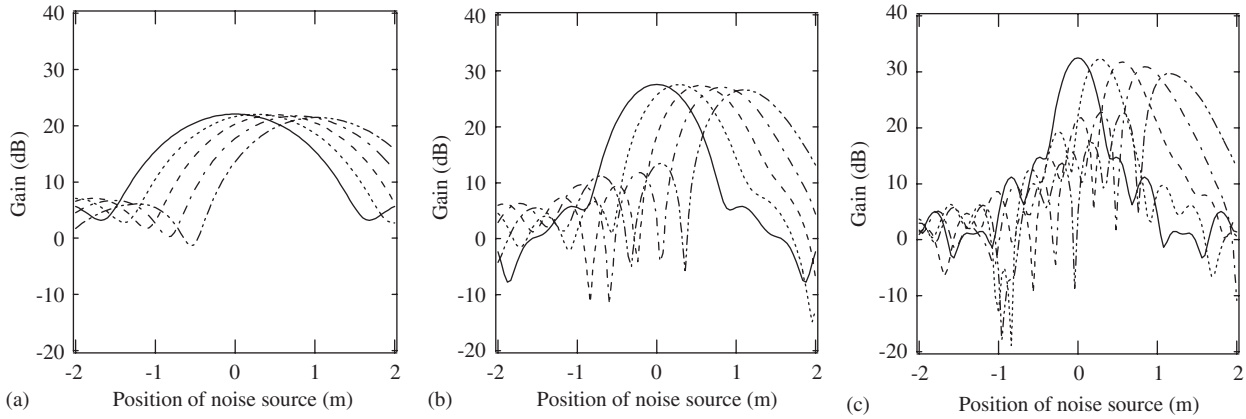

Fig. 12. Directivity patterns corresponding to different microphone positions (—, $\triangle z = 0\,\mathrm{mm}$; ....., $\triangle z = 30\,\mathrm{mm}$; – – –, $\triangle z = 60\,\mathrm{mm}$; – · – · –, $\triangle z = 90\,\mathrm{mm}$; – · · – · · –, $\triangle z = 120\,\mathrm{mm}$). (a) 1 kHz, (b) 2 kHz, (c) 4 kHz.

which is sufficient for full-scale field tests. Furthermore, nine microphones were arranged in the vertical direction near the focus at intervals of 30 mm [6].

If a microphone is located near the near-focus with an offset Δz in the vertical direction, the directivity pattern shifts in the negative direction of z by an amount of $\alpha\Delta z$, where α depends on the mirror geometry. This is because the sound path length $R_m + R_s$ is approximately constant for all points on the surface S, with

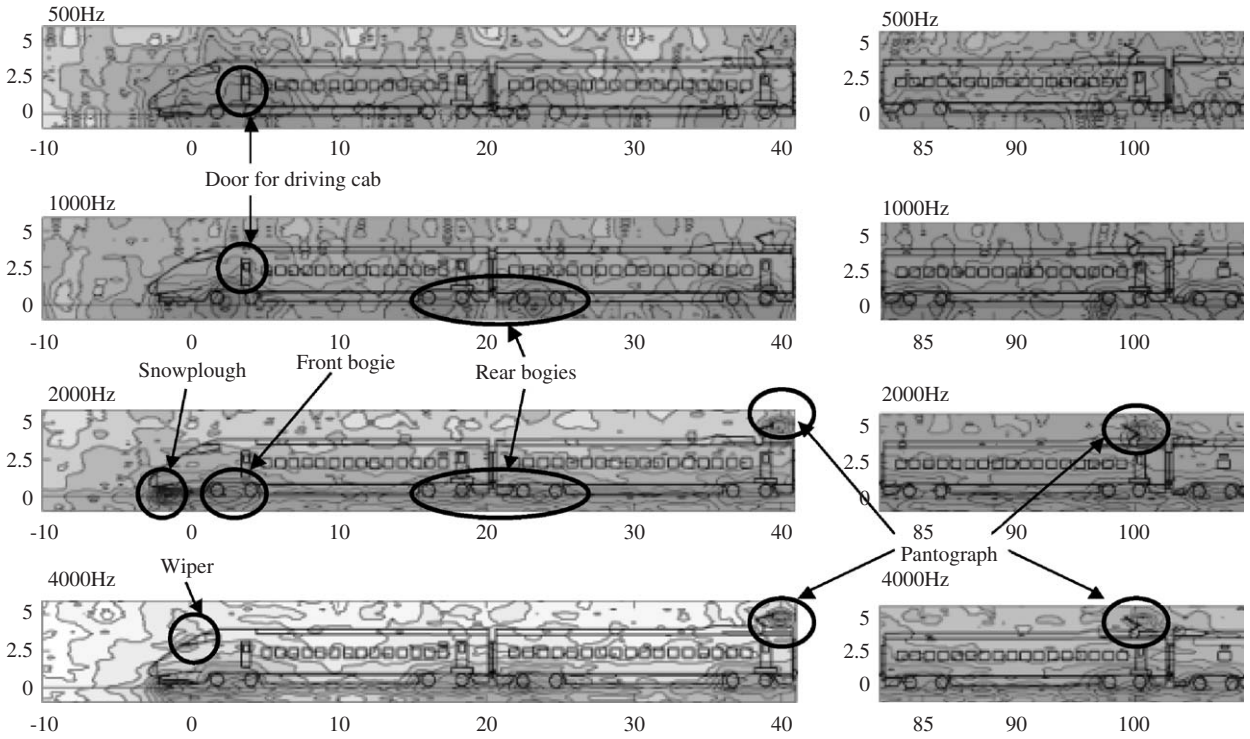

Fig. 13. Noise source distribution obtained by measurement with acoustic mirror.

respect to the offset microphone position $z = \Delta z$ and the corresponding source position $z = -\alpha\Delta z$. The calculated directivity patterns corresponding to different microphone positions at different frequencies are shown in Fig. 12. It is found that the directivity pattern shifts in the opposite direction of the microphone position, while keeping the gain factor and resolution width almost constant up to 2 kHz. At the frequency of 4 kHz or over, the gain factor and resolution width depend on microphone positions. However, it does not appear to cause a serious error as far as can be seen from the results shown in the next section. Thus, if the noise from a train passing by is measured with the acoustic mirror with plural microphones arranged near the near-focus in the vertical direction, a two-dimensional noise source map can be obtained.

In the field test, the distance between the mirror and the rail was 6.46 m, which is a little longer than the focal distance of the mirror, because of the restriction of the landform. In this case, the factor α equals 10.0, thus the measurement area covers the range $-1.2 < z < 1.2$ (m), where $z = 0$ denotes the height of the mirror centre. The measurements were performed four times at different heights of the mirror positions in order to obtain the noise source distribution on the whole train set (see Fig. 13). Typical train speed was 270 km/h and the measured values were averaged during the travel distance of about 1.6 m by every 0.37 m step.

3.2. Results of field test

Fig. 13 shows noise source maps obtained by the field test. At the frequency of 500 Hz or over, the resolution of the apparatus is sufficiently high, at high frequencies in particular, so that they provide some qualitative information about noise sources of Shinkansen trains at each frequency band. Here it should be noted that noise source maps at different frequency bands cannot be compared with each other quantitatively because the characteristics of the acoustic mirror depend on the frequency. The train used in the field test was not the same as that used in the wind tunnel test but similar to it in construction. The following results were obtained from these figures:

(a) The noise source at the front bogie of the leading car was much stronger than that at other bogies. On the other hand, the rail vibration, which was measured in the same test, corresponding to the front bogie of the

leading car was almost the same as that corresponding to other bogies. Thus, it was concluded that the aerodynamic noise dominates the wheel/rail noise at the front bogie of the leading car.

(b) The aerodynamic noise from the lower part of the leading car, which is probably caused by the shear layer at the snowplough, dominates the noise from the front bogie at the frequency of 2 kHz or over.

(c) The door for the driving cab generates a strong noise source at frequencies 500–1000 Hz.

(d) The pantograph head is the most dominant noise source at the front pantograph. On the other hand, the knee of the frame is the most dominant in the rear pantograph at some frequencies.

(e) Noise seems to be emitted from the wiper at 4 kHz.

Most of these results show the same tendencies as those of the wind tunnel test, which prove its validity, at least qualitatively. The results of field tests will be compared quantitatively with those of wind tunnel tests in the future work.

4. Concluding remarks

The principle of the acoustic mirror was discussed theoretically. A method for estimating the aerodynamic noise generated by each part of trains quantitatively was proposed on the basis of the wind tunnel test data measured with an acoustic mirror. Wind tunnel tests using a 1/5 scale Shinkansen train model were performed, by which the validity of the method was confirmed and were shown the contribution of individual noise sources of Shinkansen train to the noise level at a point 25 m away from the track. The results of the field test showed a good agreement with those of the wind tunnel tests.

References

[1] Y. Moritoh, Y. Zenda, K. Nagakura, Noise control of high-speed Shinkansen, *Journal of Sound and Vibration* 193 (1) (1996) 319–334.

[2] T. Kitagawa, K. Nagakura, Aerodynamic noise generated by Shinkansen cars, *Journal of Sound and Vibration* 231 (3) (2000) 913–927.

[3] T. Maeda, Y. Kondo, RTRI's Large-scale low-noise wind tunnel and wind tunnel tests, Quarterly Report of RTRI, Vol. 42(2), 2001, pp. 65–70.

[4] R. Sen, Interpretation of acoustic source maps made with an elliptic-mirror directional microphone system, in: *Second AIAA/CEAS Aeroacoustics Conference*, Paper No. 96-1712, 1996.

[5] W. Dobrzynski, et al., Airframe noise studies on wings with deployed high-lift devices, in: *Fourth AIAA/CEAS Aeroacoustics Conference*, Paper No. 98-2337, 1998.

[6] K. Nagakura, Y. Zenda, Noise source visualization of rolling noise based on acoustic mirror measurements, *Proceedings of the Internoise 2003*, N999, 2003.